

# Thermally and Oxidatively Stable Polymer Electrolyte for Lithium Batteries Enabled by Phthalate Plasticization

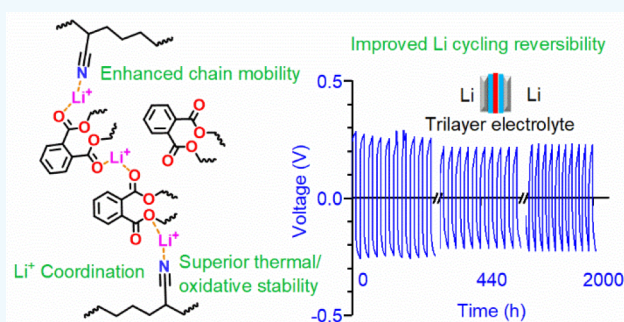
Yineng Zhao<sup>†</sup> and Wyatt E. Tenhaeff<sup>\*,‡</sup>

<sup>†</sup>Materials Science Program and <sup>‡</sup>Department of Chemical Engineering, University of Rochester, Rochester, New York 14627, United States

## Supporting Information

**ABSTRACT:** Hydrogenated nitrile butadiene rubber (HNBR) blended with lithium bis(trifluorosulfonyl)imide (LiTFSI) has been shown to be stable up to 5.3 V vs Li/Li<sup>+</sup>, making it a promising solid polymer electrolyte material for state-of-the-art high voltage cathodes. However, its relatively low room temperature ionic conductivity ( $3.6 \times 10^{-8}$  S cm<sup>-1</sup>) limits its application in practical lithium battery cells. To address this issue, phthalate esters were selected as plasticizers to improve the conductivity. The low volatility, low flammability, outstanding thermal stability, and expected high oxidative stability of phthalates make them a compelling class of plasticizers for HNBR-based polymer electrolytes. A homologous series of dialkyl phthalate esters blended with HNBR/LiTFSI was studied. The oxidation potential of the plasticized HNBR/LiTFSI exceeded 5.2 V vs Li/Li<sup>+</sup>, demonstrating that phthalates do not substantially compromise the oxidative stability. The conductivity of the electrolyte (N/Li = 5) was  $4.4 \times 10^{-5}$  S cm<sup>-1</sup> at 70 °C. FTIR revealed that phthalate esters not only increase segmental mobility of the polymer chains but also participate in the solvation of lithium salt by coordinating Li<sup>+</sup>. Electrochemical impedance analysis showed that a resistive interface developed between HNBR-based electrolytes and lithium metal, indicating a chemical incompatibility between HNBR and lithium metal. However, this problem was readily addressed through a laminated electrolyte structure where a layer of PEO/LiTFSI physically separated plasticized HNBR/LiTFSI from direct contact with lithium metal. The effectiveness of this structure was confirmed by over 2000 h of reversible galvanostatic cycling of symmetric lithium metal electrodes at 70 °C.

**KEYWORDS:** polymer electrolyte, solid-state battery, oxidative stability, battery safety, FTIR, ionic transport, hydrogenated nitrile butadiene rubber, phthalate ester



## INTRODUCTION

As adoption of electric vehicles (EVs) has increased, safety concerns over lithium ion battery technology has grown more acute.<sup>1,2</sup> Over the past several years, there have been a number of highly publicized episodes of lithium ion battery fires in consumer electronics, electric vehicles, and other propulsion devices.<sup>3,4</sup> Safety is likely to remain an ongoing challenge in lithium ion batteries given their reliance on flammable and volatile aprotic liquid electrolytes. Lithium batteries that replace the flammable liquid electrolytes with solid-state lithium ion conductors are widely regarded as the ultimate solution to lithium battery safety.<sup>5</sup> Moreover, it is believed that solid-state electrolytes will enable safe, reversible cycling of Li metal, which offers a 10-fold increase in specific energy relative to conventional graphite intercalation anodes, ultimately translating to longer-range battery packs for electric vehicles.<sup>6,7</sup>

Several material classes have been explored for solid-state lithium ion conduction; these materials and their properties are assessed in several recent review articles.<sup>7–9</sup> Ceramic lithium conductors, such as Li<sub>7</sub>La<sub>3</sub>Zr<sub>2</sub>O<sub>12</sub> (LLZO) have unity transference number, impressive oxidative and thermal stability but

suffer from difficult fabrication and high processing costs.<sup>10,11</sup> On the other hand, sulfide electrolytes, like Li<sub>7</sub>P<sub>3</sub>S<sub>11</sub> and Li<sub>9.54</sub>Si<sub>1.74</sub>P<sub>1.44</sub>S<sub>11.7</sub>Cl<sub>0.3</sub>, have high ionic conductivities surpassing those of conventional liquid electrolytes; however, they are moisture- and air-sensitive and have narrow electrochemical stability voltage windows.<sup>12,13</sup> In contrast, lithium-conductive solid polymer electrolytes (SPE) offer low processing costs and the ability to readily infiltrate composite electrodes, intimately contacting the active charge storage particles for efficient electrode utilization.<sup>14</sup> Their compliant mechanical properties also allow them to accommodate volume changes associated with lithium insertion/deinsertion.

In polymer electrolytes, the lithium salt must dissolve into the solid bulk, and ions are transported through the segmental motion of the polymer chains. Poly(ethylene oxide) (PEO)

**Special Issue:** Young Investigator Forum

**Received:** October 16, 2019

**Accepted:** December 11, 2019

**Published:** December 20, 2019

mixed with a lithium salt is the archetypical polymer electrolyte.<sup>15</sup> The existence of oxygen atoms in the polymer backbone and the absence of pendant groups endows it with outstanding flexibility.<sup>16</sup> In addition, the lone pairs of the oxygen atoms can coordinate Li<sup>+</sup>, which is necessary for disassociation of the lithium salt.<sup>17</sup> Due to its relatively high conductivity among SPEs, numerous modifications of PEO-based electrolytes have been explored, yet their low oxidative stability limits their pairing to relatively low-voltage cathodes such as LiFePO<sub>4</sub> (<4 V).<sup>15</sup> The inferior oxidative stability is associated with the ether linkage of PEO, creating an intractable problem where the linear polyether is necessary for high segmental mobility and ionic conductivities but also limits oxidative stability. The thermal stability of PEO is also problematic.<sup>18,19</sup>

These drawbacks significantly limit the competitiveness of polymer electrolytes in solid-state battery technology. For compatibility with state-of-the-art high-voltage cathodes having charge potentials of 4.5 V vs Li/Li<sup>+</sup> and beyond (some cathodes have been developed in excess of 5 V), polymer electrolytes with oxidative stability superior to PEO are required.<sup>20,21</sup> Nitrile polymers are one alternative. Poly-(acrylonitrile) (PAN) is the simplest nitrile-based polymer, and it has been thoroughly investigated for electrochemical energy storage applications.<sup>22–26</sup> However, its high  $T_g$  (low flexibility) and semicrystallinity make it unsuitable for efficient solid-state ion transport; plasticization or gelation with low molecular weight, low viscosity components are required to achieve reasonable conductivities.<sup>14,22,25</sup> Previous research in our group proposed hydrogenated nitrile butadiene rubber (HNBR) as a candidate for high-voltage applications for its superior oxidative stability of 5.4 V vs Li/Li<sup>+</sup>.<sup>27</sup> HNBR with 40% acrylonitrile content is a well-characterized amorphous polymer, of which a slight amount of microcrystalline phase can exist only after prolonged storage at subzero temperature but quickly melt at room temperature.<sup>28,29</sup> In its copolymer structure (shown in Figure S1), the alkyl segment acts as an internal plasticizer to increase segmental mobility and suppress crystallization. This polymer readily dissolves lithium bis-(trifluoromethane)sulfonimide (LiTFSI) salt and has high thermal stability (stable up to 490 °C in N<sub>2</sub>).

However, the conductivity of HNBR/LiTFSI ( $7.2 \times 10^{-6}$  S/cm at 70 °C) is still the most significant challenge preventing its application in practical batteries.<sup>27</sup> Introducing small molecule plasticizers is a potential strategy to increase segmental mobility of the polymer chains and lower  $T_g$ , but these materials should be involatile, nonflammable, and oxidatively stable such that the advantages of HNBR are not compromised. A variety of plasticizers, such as ethylene carbonate (EC), propylene carbonate (PC), and dimethyl carbonate (DMC) have been investigated with different polymers.<sup>22,30,31</sup> However, they are not suitable plasticizers for HNBR/LiTFSI because of their relatively high HOMOs and volatility (physical properties reported in Table S1). In this study, HNBR/LiTFSI was plasticized by three representative phthalate esters of varying alkyl chain length—diethyl *o*-phthalate (DEP), di-*n*-butyl *o*-phthalate (DBP), and di-*n*-octyl *o*-phthalate (DOP). Their chemical structures are shown in Figure S1. The class of phthalate esters is interesting because their calculated HOMOs are lower than conventional organic carbonates, suggesting that they should have a higher oxidation potential.<sup>32–35</sup> In addition, they have wide liquid-phase windows in excess of 300 °C, remaining liquid at subambient

temperatures (important for cold-start applications in EVs) and at high temperatures, which widens the practical temperature range over which they can be utilized.<sup>36</sup> They also have higher flashpoints than both linear and cyclic organic carbonates, suggesting that they will be less flammable.<sup>36</sup> Finally, they are common, widely used, low-cost plasticizers used extensively in the plastics industry, and they have been previously shown to be compatible with HNBR, albeit not in an electrolyte application with dissolved Li salts.<sup>37,38</sup> Key physical properties of these phthalate esters are compared in Table S1.<sup>32–38</sup> Although a few reports introduce phthalates as plasticizers for PEO-based polymer electrolytes, none of them discuss how their high oxidative stability or low volatility can be exploited to develop practical polymer electrolyte for utilization at elevated temperature.<sup>39–41</sup> Herein, the phthalate-plasticized HNBR/LiTFSI electrolytes are thoroughly characterized spectroscopically, thermally, and electrochemically. The influence of alkyl-chain length of phthalates on thermal and electrochemical properties are highlighted, and the potential utility of these formulation in electrochemical cells is demonstrated.

## ■ EXPERIMENTAL SECTION

**Sample Preparation and Chemical Analysis.** HNBR with a composition of 40 wt % acrylonitrile was kindly supplied as a gift from Zeon Chemicals. PEO (MW = 600 000 g mol<sup>-1</sup>) was purchased from Acros Organics. Battery-grade LiTFSI was purchased from TOB New Energy. Anhydrous acetone and acetonitrile (both >99% purity) were purchased from Fisher Scientific. Phthalate esters were purchased from Alfa Aesar. All chemicals were used as received.

The appropriate masses of HNBR and LiTFSI were mixed such that the molar ratio of N in acrylonitrile residues to Li<sup>+</sup> in LiTFSI was 5:1 (N/Li = 5). The materials were dissolved in acetone and cast into a PTFE mold. The solution was then dried in an N<sub>2</sub> blanketing purge flow at 50 °C for 24 h, resulting in a free-standing HNBR/LiTFSI polymer electrolyte membrane denoted by HNBR/LiTFSI. To incorporate phthalate plasticizers, the necessary mass was predissolved in acetone prior to the dissolution of HNBR and LiTFSI, and the same solution casting method was used. DEP weight fractions of 10%, 20%, and 30% (HNBR/LiTFSI/wt % DEP) were selected to study the influence of plasticizer concentration on the performance of the electrolytes. Additionally, samples containing DBP and DOP with the plasticizer loading fixed at 20 wt % (HNBR/LiTFSI/20% DBP and HNBR/LiTFSI/20% DOP) were also prepared and compared with HNBR/LiTFSI/20% DEP to study the impact of alkyl chain length on a variety of properties. All membranes of HNBR-based electrolytes were transparent indicating a single phase. For the PEO-based electrolytes (PEO/LiTFSI), acetonitrile was substituted for acetone and the molar ratio of oxygen atoms in ethylene oxide residues to Li<sup>+</sup> in LiTFSI was 10:1 (O/Li = 10). All solution preparation was conducted in an Ar-filled glovebox with H<sub>2</sub>O and O<sub>2</sub> concentrations less than 0.1 ppm, respectively. After casting the membranes in inert N<sub>2</sub>, they were stored in the gloveboxes prior to further characterization.

Fourier transform infrared spectroscopy (FTIR) was collected on a Bruker Tensor27 spectrometer employing an attenuated total reflectance (ATR) unit with a monolithic diamond crystal and 45° incident angle (Specac GoldenGate). Data was collected from 650 to 4000 cm<sup>-1</sup> with a 4 cm<sup>-1</sup> resolution using a DTGS detector. A total of 64 scans were integrated to improve the signal-to-noise ratio.

**Thermal Analysis.** The glass transition temperatures and potential phase transitions of the polymer electrolytes were characterized using differential scanning calorimetry (DSC, TA Instruments Q2000). All samples were loaded into hermetically sealed DSC pans inside the Ar-filled glovebox. The characterization protocol consisted of ramping the temperature to 100 °C, holding for 20 min to reach thermal equilibrium, then cooling to -70 °C and

finally heating back to 250 °C. The DSC furnace was purged with N<sub>2</sub> throughout the test, and all temperature ramps were 10 °C/min. Thermal transitions were analyzed in the second heating step to 250 °C.

Thermogravimetric analysis (TGA) was conducted on a TA Instrument Discovery TGA unit to characterize evaporation and decomposition in the samples. Samples were loaded into platinum pans and heated from 40 to 550 °C at 20 °C/min in pure N<sub>2</sub> or O<sub>2</sub> environments.

**Ionic Transport.** Electrochemical impedance spectroscopy was used to determine the conductivity of each sample (Solartron 1260 frequency response analyzer). Inside the glovebox, samples were assembled into a custom Swagelok cell constructed of poly-(tetrafluoroethylene) (PTFE) having a pair of stainless-steel blocking electrodes. They were then removed from the glovebox and loaded into a temperature-controlled chamber (Tenney Jr.). A 10 mV AC perturbation voltage was applied over a frequency range from 3 MHz to 100 mHz. A micrometer screw gauge was used to measure sample thicknesses after the EIS test to account for potential thickness change due to creep during high-temperature testing.

To investigate the Li<sup>+</sup> transference number (*t*<sub>+</sub>), the electrolyte membrane was sandwiched between two lithium metal electrodes in a coin cell. After thermally equilibrating the cell 70 °C, a DC voltage of 10 mV was applied and the initial current *I*<sub>0</sub> was recorded. After approximately 4000 s, the steady-state current *I*<sub>ss</sub> was established and recorded at 70 °C. For PEO/LiTFSI and HNBR/LiTFSI, the steady-state currents were recorded after 2000 and 8000 s, respectively. The plasticized polymer electrolytes are designed to operate at elevated temperatures to compensate for lower ionic conductivity, and it is important to understand their transport properties and electrochemical stability at high temperatures. A BioLogic SP-200 potentiostat was used for these tests.

**Electrochemical Stability.** Linear scanning voltammetry (LSV) and impedance evolution experiments were performed at 70 °C (BioLogic SP-200). For the LSV test, stainless steel was the working electrode while lithium metal was the counter and reference electrode. Oxidative stability is characterized by scanning the working electrode from the open-circuit voltage (OCV) to 6 V vs Li/Li<sup>+</sup> at 1 mV/s. For the impedance evolution, the studied polymer electrolytes were assembled with lithium metal symmetric electrodes in coin cells and stored at 70 °C. EIS was conducted at designated intervals at 70 °C to analyze the impedance evolution. The interfacial resistance was extracted through an equivalent circuit modeling of the Nyquist plot.

To further study the practical performance of the material, the polymer electrolytes were assembled with lithium metal symmetric electrodes in coin cells and maintained at 70 °C for plating/stripping tests. The laminated multilayer electrolyte with the PEO protective layers was prepared by pressing the two free-standing membranes together at ambient temperature inside the glovebox. During the test, a cell is cycled at 100 μA/cm<sup>2</sup> under 70 °C with 1 h charging and 1 h discharging for each cycle using a battery cycler (Neware, Model CT-ZWJ-4'S-T-1U).

## RESULTS AND DISCUSSIONS

**Infrared Spectroscopy.** The complete mid-infrared spectra for HNBR, HNBR/LiTFSI, and HNBR/LiTFSI plasticized with various phthalate esters and weight loadings are provided in Figure S2. The spectrum of HNBR is relatively simple. The stretch modes of the methylene groups in the polymer backbone reside from 3000 to 2800 cm<sup>-1</sup>, C≡N stretch of the nitrile group occurs at 2236 cm<sup>-1</sup>, and methylene bending modes are at 1465 cm<sup>-1</sup>.<sup>27</sup> Upon adding LiTFSI, strong, prominent absorbances associated with the TFSI anion appear in the range from 1400 to 1000 cm<sup>-1</sup>.<sup>42</sup> After adding phthalates as plasticizers, vibrational modes of “C=O” from 1770 to 1650 cm<sup>-1</sup> and “C–O–C” from 1325 to 1255 cm<sup>-1</sup> emerge. These vibrational modes are characteristics of ester groups in phthalates, indicating that phthalates are incorpo-

rated into the polymer electrolyte. Figure S2b shows the FTIR spectra of HNBR/LiTFSI with an increasing concentration of DEP. An increase in the peak intensity of modes “C = O” and “C–O–C” is observed as expected.

In this work, “C–O–C” band was selected to analyze the interaction between phthalates and Li<sup>+</sup>. Compared to the carbonyl stretch vibrational modes shown in Figure S3, where the “C=O–Li<sup>+</sup>” peak (1701 cm<sup>-1</sup>) is convoluted with the strong “C=O” peak (1722 cm<sup>-1</sup>), the interaction of Li<sup>+</sup> with the “C–O–C” mode is readily discernible in the spectra. Therefore, to understand the effect of phthalates upon the solvation of LiTFSI in HNBR, the details of “C–O–C” stretching mode in the fingerprint area are highlighted in parts a and b of Figure 1, as the phthalate composition and

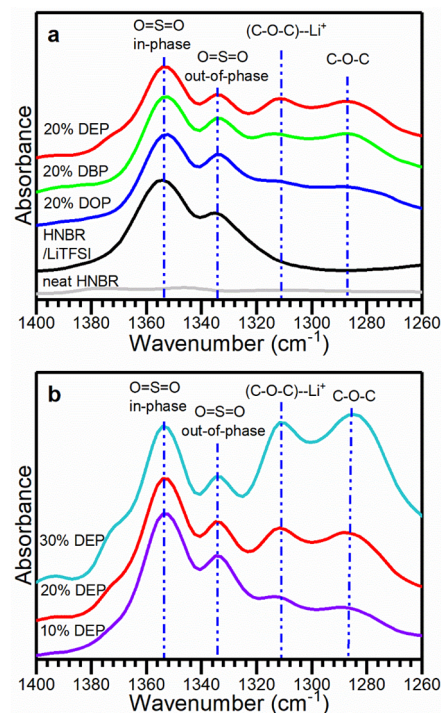


**Figure 1.** Magnified FTIR spectra from 1400 to 1260 cm<sup>-1</sup> of (a) HNBR/LiTFSI with various phthalate plasticizers, HNBR/LiTFSI, and neat HNBR; (b) HNBR/LiTFSI with varying DEP concentrations. For all compositions containing LiTFSI, N/Li = 5. The spectra are offset vertically.

concentration are varied, respectively. The peak of “O = S=O” in-phase stretching of TFSI<sup>-</sup> at 1354 cm<sup>-1</sup> is exhibited in both figures; it is a convenient baseline peak since it is unaffected by the incorporation of phthalate.<sup>42</sup> Two peaks emerge after incorporating DEP into the electrolyte. The absorption band at 1286 cm<sup>-1</sup> is identified as “C–O–C” stretching,<sup>43</sup> which is shifted relative to its value of 1272 cm<sup>-1</sup> in neat DEP e (spectrum provided in Figure S4 with other phthalates). A similar phenomenon was also observed in other ester systems by Sim et al. after introducing lithium salt.<sup>44</sup> Another peak at 1311 cm<sup>-1</sup> is also observed and grows with phthalate (DEP) concentration (Figure 1b). Interestingly, neither DEP (Figure S5) nor the HNBR/LiTFSI complex (Figure 1a) shows infrared absorption at this frequency, suggesting an assignment due to the interaction between Li<sup>+</sup> and ester groups. Therefore, this new peak is reasonably assigned to a vibrational mode of coordinated “C–O–C” group with Li<sup>+</sup>, marked as “(C–O–

C)–Li<sup>+</sup>. The presence of the “(C–O–C)–Li<sup>+</sup>” peaks for all phthalate-plasticized sample with different alkyl-chain length, shown in Figure 1a, indicates that phthalates not only act as plasticizer but coordinate the lithium ions. An expected trend is observed in Figure 1b, where the absorbances of the ester vibrational modes increase with increasing phthalate loading—consistent with Beer’s Law.<sup>45</sup>

The nitrile stretch modes as a function of phthalate composition and concentration are magnified in parts a and b of Figure 2, respectively. In Figure 2a, upon adding LiTFSI,

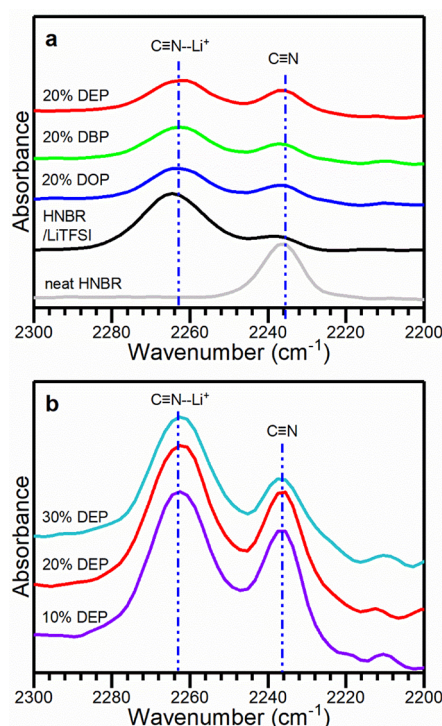


**Figure 2.** Magnified FTIR spectra from 2300 to 2200  $\text{cm}^{-1}$  of (a) HNBR/LiTFSI with various phthalate plasticizers, HNBR/LiTFSI, and pure HNBR; (b) HNBR/LiTFSI with varying DEP concentrations. For all compositions containing LiTFSI, the N/Li molar ratio is 5/1. The spectra are offset vertically.

the peak area of the “free” nitrile at 2236  $\text{cm}^{-1}$  decreases upon adding LiTFSI, while a new mode emerges at 2262  $\text{cm}^{-1}$ . This new mode is the stretch of nitrile coordinated to Li<sup>+</sup>.<sup>24,27</sup> Incorporating phthalates into the system significantly reduces the peak intensity ratio of the coordinated “C≡N–Li<sup>+</sup>” to “free C≡N”, indicating that some cyano groups are released from coordination with Li<sup>+</sup>. This is attributed to the fraction of the free dissociated Li<sup>+</sup> preferentially coordinating to the phthalate ester over the nitrile groups. Interestingly, Figure 2b shows that the ratio “C≡N–Li<sup>+</sup>/C≡N” does not decrease as the phthalate loading increases; instead, it has a slight increase. This is evident after the peaks are deconvoluted—shown in Figure S6. The area ratio of the two bands increases—from 1.97 to 2.42 with DEP concentration rise from 10% to 30%. It is possible that as more ester groups are incorporated into the electrolyte, the degree of dissociation of LiTFSI increases due to an overall increased bulk permittivity due to the phthalates. This is consistent with the results in Figure 1b showing that increased concentration of coordinated Li<sup>+</sup> as the phthalate loading is increased, implying a greater degree of salt dissociation.

**Thermal Properties.** Since ionic transport in conventional polymer electrolytes is correlated to segmental mobility, the glass transition temperature ( $T_g$ ) is a critical property governing the conductivity of polymer electrolytes.<sup>46,47</sup> The  $T_g$  of all the materials prepared in this study are reported in Table 1. The  $T_g$ ’s of PEO and HNBR (with 40 wt %

**Table 1.** Thermal Properties of the Polymer Electrolytes

sample	$T_g/^\circ\text{C}$	$T_{\text{evap}}/^\circ\text{C}$ in $\text{N}_2/\text{O}_2$	$T_{\text{decom}}/^\circ\text{C}$ in $\text{N}_2/\text{O}_2$
HNBR	–24.3	–	–/402 <sup>27</sup>
PEO	–64 <sup>48</sup>	–	–/174 <sup>27</sup>
HNBR/LiTFSI	–12.4	–	449/415
PEO/LiTFSI	–39.8	–	414/184
HNBR/LiTFSI with 10% DEP	–17.5	160/–	449/–
20% DEP	–29.1	160/158	442/406
30% DEP	–36.5	160/–	449/–
20% DBP	–28.9	181/177	449/407
20% DOP	–28.5	233/223	449/414

acrylonitrile) are reported to be –64 and –24  $^\circ\text{C}$ , respectively.<sup>27,48</sup> The 40  $^\circ\text{C}$  difference in  $T_g$  of neat PEO and HNBR is an indication of the significant difference in chain mobility between PEO and HNBR. The rotational mobility of PEO is benefited by its linear structure with the coordinating oxygen incorporated in the polymer backbone. On the other hand, HNBR has strongly polarized nitrile groups “–C≡N” pendant to the main chain, leading to polar interactions and steric hindrance that limit chain mobility.

Upon addition of LiTFSI, the  $T_g$ ’s of PEO/LiTFSI (O/Li = 10) and HNBR/LiTFSI (N/Li = 5) are increased relative to their pure counterparts (see Table 1) as a consequence of physical cross-links between coordinated ions and the polymer chains. The cross-linking further hinders the mobility of polymer chains. This phenomenon is known as the compensation effect.<sup>49</sup> Therefore, developing a new polymer electrolyte requires a trade-off between the concentration of dissociated Li<sup>+</sup> and the efficiency of their transport ( $T_g$  of the polymer electrolyte).

After incorporating phthalates as plasticizers into the HNBR-based electrolytes, the  $T_g$  is significantly lowered indicating improved flexibility and mobility of polymer chains by plasticization. The increasing weight fraction of phthalates in the electrolyte leads to a lower  $T_g$ . The electrolytes with 10%, 20%, and 30% DEP have  $T_g$  of –17.5, –29.1, and –36.5  $^\circ\text{C}$ , respectively. The lowest  $T_g$  (–36.5  $^\circ\text{C}$ ) of HNBR-based electrolyte is achieved by adding 30% DEP; however, it is still 3.3  $^\circ\text{C}$  higher than the  $T_g$  of plasticizer-free PEO/LiTFSI electrolyte (O/Li = 10). The inclusion of 30% plasticizer results in a morphology more consistent with a gel, lacking sufficient mechanical strength for a self-standing membrane. Measures such as introducing ceramic fillers, even ceramic electrolytes, can be explored to enhance the mechanical strength of the polymer electrolytes with higher plasticizer concentration in future.<sup>50,51</sup> To limit the scope of this study, 20% plasticizer in the total weight is selected as an optimal concentration and maintained for comparison between different phthalate species. Changing the composition of the phthalates has a much smaller effect on  $T_g$ , but it is observed

that the longer alkyl chains slightly result in higher  $T_g$ . This is consistent with a previous report on the influence of chain-length on plasticization efficiency, which is explained by a reduced polymer-plasticizer interaction due to dilution of the ester groups.<sup>52</sup> DSC further confirmed that the absence of crystallinity or any other phase transient peaks in the plasticized HNBR electrolyte over the temperature ranging from  $-70$  to  $250$  °C.

Thermogravimetry was used to analyze the thermal and thermo-oxidative stability of the investigated samples in  $N_2$  and  $O_2$  environments, respectively. The onset temperatures of significant thermal processes can be found in Table 1. For plasticized HNBR/LiTFSI, there are two steps of weight loss during heating (shown in Figure 3)—evaporation of phthalates

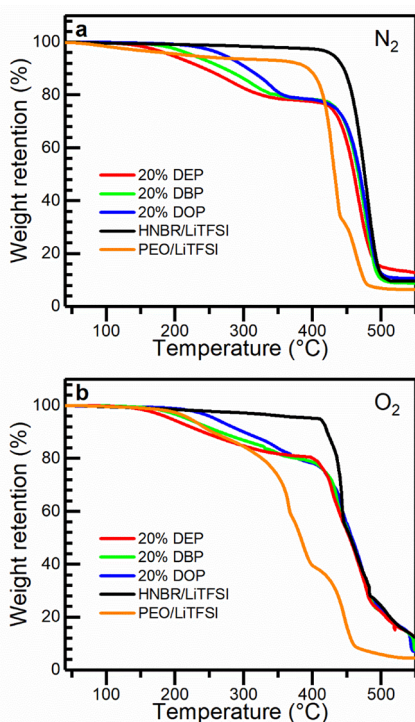


**Figure 3.** Thermogravimetric analysis of HNBR/LiTFSI electrolytes plasticized with several phthalate esters, nonplasticized HNBR, and PEO-based electrolytes in pure (a)  $N_2$  and (b)  $O_2$  environments with a temperature ramp rate of  $20$  °C/min.

between  $150$  to  $360$  °C and decomposition of HNBR/LiTFSI above  $400$  °C. The onset decomposition temperature ( $T_{decom.}$ ) of HNBR/LiTFSI under  $N_2$  is  $449$  °C while that of PEO/LiTFSI is  $414$  °C. Switching to pure  $O_2$  atmosphere, the oxidation of PEO begins at  $184$  °C, while HNBR withstands up to  $415$  °C. These results demonstrate the superior thermal and thermo-oxidative stability of HNBR-based electrolytes.

In a full battery, gas release is a serious safety concern.<sup>53</sup> Commercial liquid electrolytes that utilize diethyl carbonate (DEC) and/or dimethyl carbonate (DMC) are unsuitable plasticizers for polymer electrolytes because of their high flammability and volatility. Their low boiling points (b.p.) increase the risk of gas release at elevated temperature, and their low flash points represent high flammability (shown in Table S1). In contrast, phthalate-plasticized electrolytes exhibit superior stability at high temperatures. Figure 3a demonstrates that at  $120$  °C (higher than the b.p. of DMC), weight losses of all electrolytes containing plasticizers are negligible ( $<0.5\%$ ).

After heating to  $150$  °C (higher than the bp of DEC), the weight losses of DBP and DOP-plasticized HNBR electrolytes are still insignificant ( $<0.5\%$ ). In the DEP-plasticized samples, the weight loss is less than  $2\%$ . Remarkably, even in pure  $O_2$  environment (Figure 3b), the plasticized HNBR/LiTFSI electrolytes show no decomposition or oxidation before  $400$  °C and the onset temperatures of evaporation are similar to those in  $N_2$ . In conclusion, phthalates-plasticized HNBR/LiTFSI electrolytes exhibit superior thermal and thermo-oxidative stability. Introducing phthalates into the polymer electrolytes does not significantly compromise the thermal and thermo-oxidative stability of the polymer electrolyte and employing the polymer electrolytes at elevated temperature is feasible.

**Ionic Transport.** A typical Nyquist plot of the polymer electrolyte membrane between two blocking electrodes is shown in the inset of Figure 4, along with the equivalent circuit

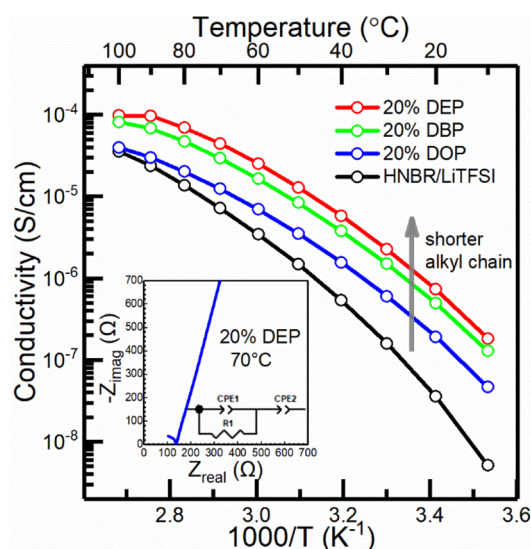


**Figure 4.** Temperature dependence of lithium ion conductivity in a series of plasticized HNBR/LiTFSI electrolytes. A typical corresponding Nyquist plot along with the equivalent circuit used for modeling is provided in the inset.

used for modeling. Constant phase elements (CPEs) were used to describe the nonideal capacitances in the system, which is standard practice in the field.<sup>54,55</sup> The equivalent circuit consisted of  $CPE_1$  in parallel with the resistor  $R_1$ ,  $CPE_1//R_1$ , to describe the bulk impedance of electrolyte in series with  $CPE_2$ , which described the double-layer capacitance due to charge accumulation at the blocking electrodes. In the Nyquist plot,  $CPE_1//R_1$  describes the partial semicircle at high frequencies (left of the curve), and  $CPE_2$  forms a straight line at low frequency with an angle to the imaginary axis. The full semicircle associated with the electrolyte bulk is not observed experimentally because its characteristic frequency is beyond the frequency range of the characterization equipment. However, the presence of only one semicircle (partially developed) suggests that the electrolyte bulk behaves as a homogeneous mixture.

$R_1$  is the resistance of the bulk electrolyte obtained from equivalent circuit modeling.  $R_1$  was used along with the thickness ( $d$ ) and area ( $A$ ) of the electrolyte to determine conductivity ( $\sigma$ ) using the following relationship:

$$\sigma = \frac{d}{A \cdot R_1} \quad (1)$$

The temperature dependence of the conductivities of HNBR/LiTFSI plasticized with the three different phthalates at 20 wt % is shown in Figure 4. The curvature of the plot suggests that the Vogel–Tammann–Fulcher (VTF) relationship should be applied to these polymer electrolytes, shown in the following equation:<sup>56,57</sup>

$$\sigma = Ae^{-E_a/R(T-T_0)} \quad (2)$$

where  $A$  is a pre-exponential factor,  $E_a$  is pseudo activation energy,  $R$  is the ideal gas constant, and  $T$  is absolute temperature.  $T_0$  in this equation is the Vogel temperature—equal to the glass transition in ideal gases and typically taken as 50 °C below the glass transition temperature of the polymer electrolyte.<sup>49,58</sup> It demonstrates that the conductivity of polymer electrolytes is correlated to the mobility of polymer chains, which is characterized by  $T_g$ .<sup>49</sup> All plasticized electrolytes have higher conductivity than the nonplasticized HNBR/LiTFSI. It is noted that the phthalate with the longer alkyl chains generally gives lower conductivity. However, the  $T_g$  of these polymer electrolytes is too similar to explain the conductivity trend. The FTIR results revealed that the role of the phthalates is not only plasticization. Rather, they also contribute to the  $\text{Li}^+$  solvation and dissociation of LiTFSI and enhance conductivity through their diffusivity. Phthalate esters with longer alkyl chains (e.g., DOP) have higher viscosity and lower permittivity, leading to less efficient ionic transport (Walden's rule) and a lower degree of salt disassociation.<sup>37,59–61</sup> This explains the distinct conductivity dependence on the plasticizer alkyl chain length. It is noted that the conductivity curves are smooth and continuous, indicative of ion transport in amorphous materials. This is additional evidence that the phthalate plasticizers are miscible in the polymer electrolyte, resulting in a single-phase over the temperature range of the experiments.

The conductivities of HNBR/LiTFSI as a function of DEP concentration is shown in Figure 5. The result shows that an

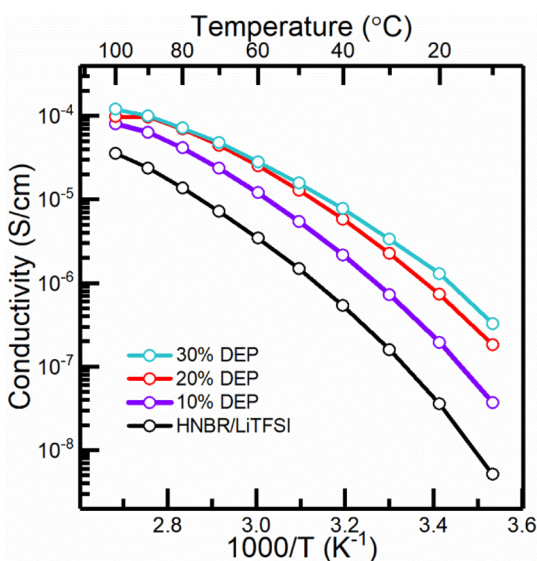


**Figure 5.** Temperature dependence of lithium ion conductivity of HNBR/LiTFSI as a function of DEP concentration.

increased amount of plasticizer leads to higher conductivity. Although the conductivities at room temperature are too low to have a practical application ( $1.8 \times 10^{-7} \text{ S cm}^{-1}$  for HNBR/LiTFSI/20% DEP at 20 °C), running a cell at elevated temperature should mitigate this problem. The remarkable thermal stability and limited volatility of the phthalates make this viable. For example, at 70 °C at which most following tests are conducted, the conductivities of HNBR/LiTFSI containing 0%, 10%, 20%, and 30% DEP are  $7.2 \times 10^{-6}$ ,  $2.4 \times 10^{-5}$ ,  $4.4 \times 10^{-5}$ , and  $4.8 \times 10^{-5} \text{ S cm}^{-1}$ , respectively. Although the highest value at 70 °C is achieved by incorporating 30% DEP, it is only a modest increase of 9% relative to the formulation with 20% DEP. The drawback to higher phthalate concentrations is poor mechanical properties, which are more consistent with a gel instead of a solid polymer. Hence, HNBR/LiTFSI/20% DEP was selected for further electrochemical characterization. It is interesting that the conductivity of HNBR/LiTFSI/20% DEP is  $7.3 \times 10^{-7} \text{ S cm}^{-1}$  at 20 °C—higher than that of PEO/LiTFSI (EO/Li = 10) at the same temperature, which is reported to be  $6 \times 10^{-7} \text{ S cm}^{-1}$ .<sup>62</sup> This is a result of the amorphous nature of HNBR in contrast to PEO which has a crystalline phase at room temperature that is unfavorable for ionic transport. However, PEO/LiTFSI achieves  $4 \times 10^{-4} \text{ S cm}^{-1}$  at 60 °C—an order of magnitude higher than that of HNBR/LiTFSI/20% DEP—due to the melting of the crystallites and the PEO becoming fully amorphous. The  $T_g$  of PEO/LiTFSI is lower than HNBR's despite the plasticization.

The  $\text{Li}^+$  transference number ( $t_+$ ) is another critical property of electrolytes. Low  $t_+$  leads to a severe concentration polarization of ions limiting both rate and energy density in lithium ion batteries.<sup>63,64</sup> Ideally, the transference number is unity, and ionic current is contributed entirely by  $\text{Li}^+$ . The transference numbers of conventional liquid electrolytes are usually below 0.5, indicating that the diffusivity of the anions is higher than that of  $\text{Li}^+$ .<sup>35</sup> For polymer electrolytes, however, accurate estimation of transference numbers is a challenging problem.<sup>65</sup> Several approaches have been developed over the years, but most have significant limiting assumptions, such as dilute salt concentrations and the absence of ion pairs/cluster contributions.<sup>66–68</sup> Four characterization methods have been compared, and the potentiostatic method is generally considered the most convenient to implement.<sup>69</sup> But it is complicated by overpotentials associated with interfacial layers, which is especially difficult when these interfacial layers do not fully passivate (as will be shown below for plasticized HNBR/LiTFSI).<sup>70</sup> Therefore, we do not attempt to estimate transference number, but rather report the ratio of steady-state current to initial current ( $I_{ss}/I_0$ ) in response to a 10 mV DC bias. Ultimately, this ratio is a practical quantity representing the fraction of the total current that will be carried by  $\text{Li}^+$ . The current response for HNBR/LiTFSI/20% DEP symmetrical cell with Li metal electrodes is shown in Figure 6a. Equivalent current responses for HNBR/LiTFSI and PEO/LiTFSI are provided in Figure S7. The initial current of 16.5  $\mu\text{A}$  should be contributed by the transport of both  $\text{Li}^+$  and TFSI<sup>-</sup>. However, since the electrodes are only conductive to  $\text{Li}^+$ , a concentration polarization of TFSI<sup>-</sup> is establishing over time and eventually, and the steady-state current of 11.0  $\mu\text{A}$  is completely contributed by  $\text{Li}^+$ . The current responses of PEO/LiTFSI (O/Li = 10), HNBR/LiTFSI, and HNBR/LiTFSI/20% DEP measured at 70 °C are compared in Figure 6b. The current ratios are significantly higher in the nitrile-

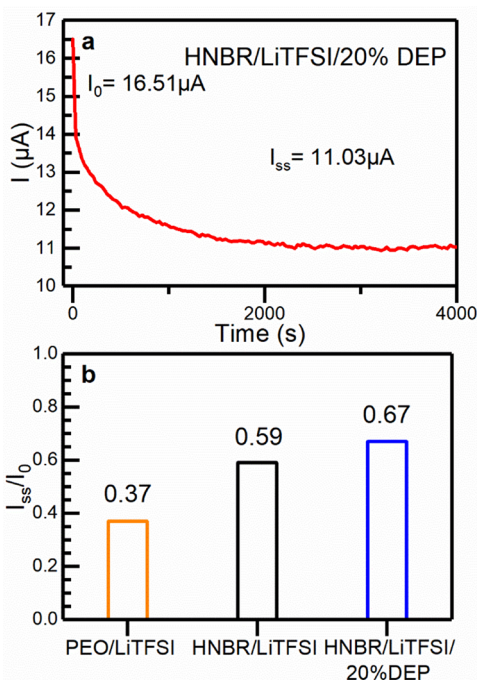


**Figure 6.** (a) Chronopotentiometry of HNBR/LiTFSI/20% DEP with lithium metal symmetrical electrodes at 70 °C, 10 mV applied voltage. (b) Comparison of  $I_{ss}/I_0$  of PEO/LiTFSI (O/Li = 10), HNBR/LiTFSI (N/Li = 5), and HNBR/LiTFSI/20% DEP (N/Li = 5) measured at 70 °C.

bearing electrolytes. It is interesting to note that the current ratio of 0.37 is in very close agreement to previously reported transference numbers for PEO/LiTFSI (O/Li = 10).<sup>71</sup> While the current ratio is smaller in PEO, the total current steady-state current is higher, due to the greater segmental mobility of PEO, leading to enhanced  $\text{Li}^+$  diffusivities. The physical processes leading to higher current ratios in both plasticized and unplasticized HNBR have not been identified and will be the subject of future studies.

**Electrochemical Stability.** The oxidative potentials of the HNBR/LiTFSI/20% DEP, HNBR/LiTFSI, and PEO/LiTFSI were characterized by linear scanning voltammetry (LSV) method and compared in Figure 7. Since the working electrode is blocking toward  $\text{Li}^+$ , the capacitance of the cell provides a flat and small current response with increasing applied voltage

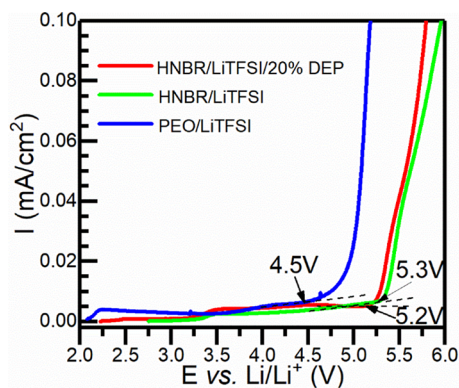


**Figure 7.** Linear sweep voltammetry of PEO/LiTFSI, HNBR/LiTFSI, and HNBR/LiTFSI/20% DEP scanned at 1 mV/s at 70 °C. Stainless steel is the working electrode.

before the onset of oxidation. The oxidative stability of the polymer electrolytes is taken at the potential (vs  $\text{Li}/\text{Li}^+$ ), where there is a significant increase in current beyond this background capacitive current. The HNBR/LiTFSI exhibits the highest oxidative voltage of 5.3 V vs  $\text{Li}/\text{Li}^+$  at the stainless steel working electrode. After blending with 20% DEP, the onset voltage is slightly reduced to 5.2 V vs  $\text{Li}/\text{Li}^+$ . Although the presence of DEP slightly lowers the onset potential of oxidation, it still maintains remarkable oxidative stability to withstand delithiated potentials of charged  $\text{LiCoO}_2$  and  $\text{LiNi}_{1-x-y}\text{Mn}_y\text{Co}_{1-x-y}\text{O}_2$  cathodes (potentials of 4.2–4.6 V vs  $\text{Li}/\text{Li}^+$ ).<sup>72</sup> Moreover, the oxidative potential of HNBR/LiTFSI/20% DEP electrolyte is 0.7 V higher than that of PEO, which is 4.5 V vs  $\text{Li}/\text{Li}^+$  under the same conditions. The oxidative potential of PEO measured by LSV method on a stainless steel working electrode is typically elevated relative to its practical voltage limit in a real battery where cathode materials have a catalytic effect on the oxidation of PEO. The retention of high oxidative stability of DEP-plasticized HNBR/LiTFSI is attributed to the low HOMO of DEP (−10.66 eV) which makes it less susceptible to oxidation and, thus, does not significantly compromise the oxidative stability of HNBR.<sup>33</sup>

To characterize the electrochemical stability of these electrolyte formulations with Li metal, the evolution of interfacial resistance of the electrolytes in direct contact with Li metal at 70 °C was monitored as a function of time using electrochemical impedance spectroscopy. The impedance data are presented as Nyquist plots in Figure 8. The four key processes that comprise the impedance spectra—the bulk

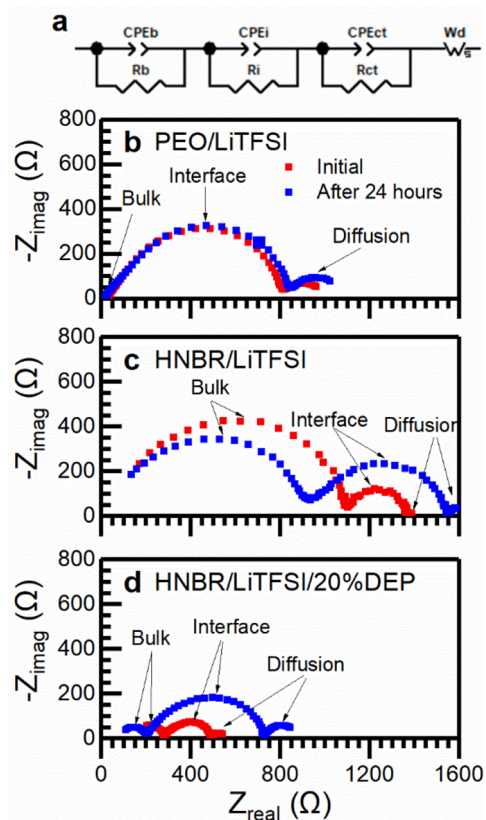


**Figure 8.** (a) Equivalent circuit used to model impedance of Li metal symmetric cells at 70 °C with impedance evolution over 24 h with (b) PEO/LiTFSI (O/Li = 10), (c) nonplasticized HNBR/LiTFSI (N/Li = 5), and (d) HNBR/LiTFSI/20% DEP (N/Li = 5) electrolytes.

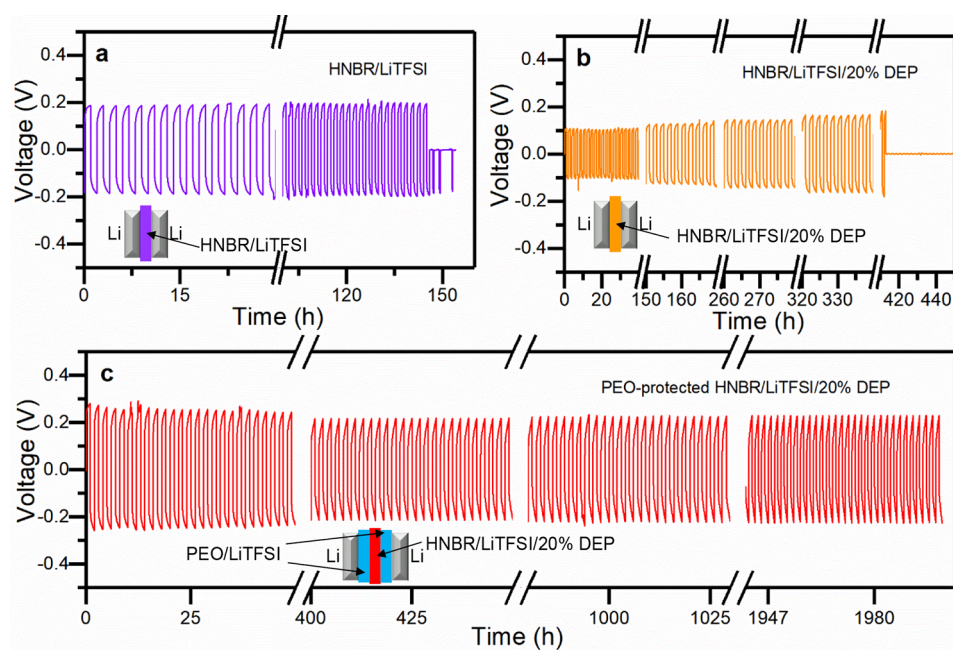


**Figure 9.** Galvanostatic cycling of Li/Li symmetric cells employing single layer electrolytes of (a) HNBR/LiTFSI and (b) HNBR/LiTFSI/20% DEP, and a laminated trilayer of (c) PEO/LiTFSI | HNBR/LiTFSI/20% DEP | PEO/LiTFSI. The current density was  $100 \mu\text{A}/\text{cm}^2$ , and the cell temperatures were regulated at  $70^\circ\text{C}$ .

electrolyte, a surface reaction layer, charge transfer at the Li interface, and diffusion—are modeled with the equivalent circuit provided in Figure 8a. The mass transport is modeled by a finite length Warburg element ( $W_d$ ) while the other three are represented by parallel RC elements, where constant phase element (CPE) are used to describe nonideal capacitances. The surface layer and the charge transfer have a similar time constant; thus, their impedance response is difficult to fully distinguish by the EIS method, and they form one depressed semicircle at intermediate frequencies in the Nyquist plot. Therefore, the impedance responses of the surface layer and the charge transfer are referred to the interfacial impedance since they both relate to the interface between lithium metal electrode and the polymer electrolyte.

The characteristic frequency of PEO/LiTFSI ( $O/\text{Li} = 10$ ) at  $70^\circ\text{C}$  is beyond the range of the potentiostat; thus, only a bulk resistance of approximately  $32 \Omega$  can be resolved through the high-frequency intercept with the real component of impedance (Figure 8b). The second semicircle at intermediate frequency is attributed to the interfacial impedance. A partial semicircle at the lowest frequencies is associated with mass transport. The interfacial resistance of PEO/LiTFSI electrolyte only increases by 3.7% in 24 h indicating a relatively stable surface layer formed on the lithium metal electrode at  $70^\circ\text{C}$ .

For the HNBR-based electrolytes (Figure 8, parts c and d), the first (left) semicircle is attributed to the electrolyte bulk. The reduction in its resistance over 24 h (decreased diameter) is likely due to a reduction in film thickness due to creep. The electrolyte HNBR/LiTFSI without plasticizer develops a very resistive interface ( $272 \Omega$ ) with lithium metal, which is reflected by the large diameter of the second semicircle in Figure 8c. After 24 h, the resistance further grows to  $611 \Omega$ , indicating the interface is not only resistive but also unstable. With 20% DEP added to the HNBR/LiTFSI (Figure 8d), the initial bulk resistance is significantly lowered from  $1102 \Omega$  to  $283 \Omega$  due to the increased conductivity. However, a resistive

interface develops, growing from  $211 \Omega$  to  $527 \Omega$  over 24 h at  $70^\circ\text{C}$ . It is slightly smaller than that of the nonplasticized one but still comparable. The resistance increase of the HNBR/LiTFSI/20% DEP and its nonplasticized counterpart are  $316 \Omega$  (150% increase) and  $339 \Omega$  (125% increase), respectively. The similar behavior of the two HNBR-based electrolytes implies similar resistive interfaces formed. It is likely due to the reduction of HNBR on the lithium surface. The presence of phthalate, which is also reactive with lithium metal, may also contribute to and accelerate the growth of this resistive layer. The impedance evolution indicates that HNBR/LiTFSI and HNBR/LiTFSI/20% DEP do not form a stable interface with lithium metal like PEO/LiTFSI. Instead, a rather resistive and unstable interface is developed, suggesting that a strategy to prevent HNBR-based electrolytes from direct contact with lithium metal is necessary for utilization in practical battery cells.

#### Plating and Stripping in Lithium Symmetrical Cells.

To assess the utility of these electrolytes in a real electrochemical system, galvanostatic plating and stripping of lithium metal in symmetrical cells were performed. Each cycle included 1 h of plating and 1 h of stripping at  $100 \mu\text{A}/\text{cm}^2$  at  $70^\circ\text{C}$ . The voltage–time profiles of plating and stripping results are shown in Figure 9. The single-layer HNBR/LiTFSI electrolyte without plasticizer, shown in Figure 9a, has a 0.19 V initial overpotential. Given the applied current, this value corresponds to about  $1500 \Omega$  resistance, which is consistent with the bulk and interfacial resistance determined previously through impedance spectroscopy. After 146 h, the sudden drop in voltage indicates short-circuiting—likely the result of lithium dendrite penetration. Before its failure, the overpotential had increased slightly to 0.20 V, possibly due to increased interfacial resistance as discussed before.

With 20% DEP embedded into the nitrile-bearing electrolyte, the initial overpotential is reduced to 0.10 V (shown in Figure 9b) corresponding to a DC resistance of  $780 \Omega$ , which

is also consistent with the previous impedance result. The short-circuiting does not occur until 413 h, nearly three times longer than the nonplasticized HNBR/LiTFSI, indicating a significantly improved cycling life. However, constant growth of overpotential during the cycling test is observed. Right before the short-circuiting, the overpotential has grown to 0.18 V—almost double its initial overpotential. Considering the nonplasticized HNBR/LiTFSI does not share this huge growth of overpotential or resistance, the increase is unlikely from the surface layer formed by HNBR and lithium metal. Instead, a role of phthalate plasticizers is implicated here. Interestingly, before the failure, the overpotential of the plasticized electrolyte becomes rather similar to that of the nonplasticized one. It suggests that the phthalate plasticizer could have been depleted by a reaction with lithium metal—likely lithium dendrites—during the Li cycling. This might contribute to the improved cycling life of the cell; the phthalate esters react quickly with the high surface area dendrites, leading to “dead” Li and overall slower propagation across the polymer electrolyte region. Nonetheless, an increased conductivity could also be part of the reason for the improvement of cycling performance since higher conductivity leads to a higher critical current of dendrite formation and suggests less aggressive dendrite propagation.<sup>73</sup>

To achieve a stable interface, a protective layer of PEO/LiTFSI was interspersed between the HNBR-based electrolyte and lithium metal on both sides. Using HNBR/LiTFSI/20% DEP sandwiched between the PEO layers, the calendar life of the plating/stripping cell is prolonged to over 2000 h (presented in Figure 9c)—no short-circuiting is detected. After a slight decrease in overpotential from 0.28 to 0.22 V in the first 140 h, the overpotentials remain remarkably stable for the duration of the test. It is worth noting that given a higher DC resistance (inferred from the overpotentials) of the laminated electrolyte than that of the single-layer plasticized HNBR/LiTFSI, the cycling life is dramatically improved which cannot be solely supported by an increased critical current for lithium dendrite formation. A possible explanation is that lithium dendrites penetrating into the middle layer are mostly consumed by a reaction with phthalate. With the protective layer of PEO on HNBR/LiTFSI/20% DEP, phthalate molecules do not react as quickly with the bulk lithium electrode. Further experimentation is required to fully elucidate the detailed mechanism responsible for this behavior.

These results demonstrate that laminated polymer electrolyte structures are an effective strategy for the incorporation of polymer electrolytes with high oxidative stability but are reductively stable against Li metal. A similar approach was also reported by Zhou et al., but plasticizer was not used.<sup>74</sup> This straightforward strategy has significant implications for lithium batteries as it allows polymers electrolytes to be designed independently for each electrode. It broadens the material choices for SPEs, which is essential considering the difficulty of achieving both extraordinary anodic and cathodic stability in organic compounds.

## CONCLUSION

The room temperature lithium ion conductivity of HNBR/LiTFSI electrolytes is enhanced by a factor of 20 through phthalate ester plasticization without significant compromise of electrochemical oxidative stability. The oxidative potential of HNBR/LiTFSI electrolytes is above 5 V vs Li/Li<sup>+</sup>, with or without phthalate plasticization. It was shown that the

phthalate esters not only plasticize the HNBR, decreasing the  $T_g$  by 17 °C with the incorporation of 20 wt % DEP, but they also participate in the coordination of Li<sup>+</sup>, which was confirmed through FTIR analysis. The phthalate-plasticized HNBR/LiTFSI electrolytes show preeminent thermal and thermo-oxidative stability up to 400 °C in both inert and oxidizing gas environments, and the evaporation of the phthalate plasticizers remain insignificant up to 150 °C. However, one important limitation of HNBR-based electrolytes is the chemical incompatibility with Li metal, resulting in a significant, continual evolution of a highly resistive interface. It was shown that a simple lamination strategy where Li-stable PEO/LiTFSI is interspersed between HNBR and Li to prevent their direct contact enables the successful cycling of Li metal. This trilayer laminated electrolyte can cycle with Li metal for over 2000 h with a stable DC resistance. Without the PEO lamination, HNBR/LiTFSI/20% DEP shows continual growth in DC resistance and has a much shorter time to failure of approximately 420 h.

## ASSOCIATED CONTENT

### Supporting Information

The following files are available free of charge. The Supporting Information is available free of charge at <https://pubs.acs.org/doi/10.1021/acsapm.9b00986>.

Chemical structure of compounds; key physical properties of phthalates and carbonates; full-scale FTIR spectra of polymer electrolytes, neat HNBR, and neat phthalates; peak analysis of IR spectra of CN groups; and chronopotentiometry of PEO/LiTFSI and HNBR/LiTFSI (PDF)

## AUTHOR INFORMATION

### Corresponding Author

\*(W.E.T.) E-mail: [wyatt.tenhaeff@rochester.edu](mailto:w Wyatt.tenhaeff@rochester.edu).

### ORCID

Yineng Zhao: 0000-0002-8899-7663

Wyatt E. Tenhaeff: 0000-0001-7132-3171

### Notes

The authors declare no competing financial interest.

## ACKNOWLEDGMENTS

The authors would like to thank the University of Rochester Materials Science Program for funding this research in part. The authors also thank Dr. Shaofei Wang, Zhuo Li, Jiawen Liu, and Ni Huo for valuable discussions.

## REFERENCES

- (1) Etacheri, V.; Marom, R.; Elazari, R.; Salitra, G.; Aurbach, D. Challenges in the development of advanced Li-ion batteries: a review. *Energy Environ. Sci.* **2011**, *4* (9), 3243–3262.
- (2) Feng, X.; Ouyang, M.; Liu, X.; Lu, L.; Xia, Y.; He, X. Thermal runaway mechanism of lithium ion battery for electric vehicles: A review. *Energy Storage Materials* **2018**, *10*, 246–267.
- (3) Wang, Q.; Ping, P.; Zhao, X.; Chu, G.; Sun, J.; Chen, C. Thermal runaway caused fire and explosion of lithium ion battery. *J. Power Sources* **2012**, *208*, 210–224.
- (4) Williard, N.; He, W.; Hendricks, C.; Pecht, M. Lessons Learned from the 787 Dreamliner Issue on Lithium-Ion Battery Reliability. *Energies* **2013**, *6* (9), 4682–4695.
- (5) Manthiram, A.; Yu, X.; Wang, S. Lithium battery chemistries enabled by solid-state electrolytes. *Nature Reviews Materials* **2017**, *2*, 16103.

- (6) Goodenough, J. B.; Park, K.-S. The Li-Ion Rechargeable Battery: A Perspective. *J. Am. Chem. Soc.* **2013**, *135* (4), 1167–1176.
- (7) Cheng, X.-B.; Zhang, R.; Zhao, C.-Z.; Wei, F.; Zhang, J.-G.; Zhang, Q. A Review of Solid Electrolyte Interphases on Lithium Metal Anode. *Advanced Science* **2016**, *3* (3), 1500213.
- (8) Xin, S.; You, Y.; Wang, S.; Gao, H.-C.; Yin, Y.-X.; Guo, Y.-G. Solid-State Lithium Metal Batteries Promoted by Nanotechnology: Progress and Prospects. *ACS Energy Letters* **2017**, *2* (6), 1385–1394.
- (9) Zhang, Q.; Liu, K.; Ding, F.; Liu, X. Recent advances in solid polymer electrolytes for lithium batteries. *Nano Res.* **2017**, *10* (12), 4139–4174.
- (10) Kerman, K.; Luntz, A.; Viswanathan, V.; Chiang, Y.-M.; Chen, Z. Review—Practical Challenges Hindering the Development of Solid State Li Ion Batteries. *J. Electrochem. Soc.* **2017**, *164* (7), A1731–A1744.
- (11) Thangadurai, V.; Narayanan, S.; Pinzaru, D. Garnet-type solid-state fast Li ion conductors for Li batteries: critical review. *Chem. Soc. Rev.* **2014**, *43* (13), 4714–4727.
- (12) Kato, Y.; Hori, S.; Saito, T.; Suzuki, K.; Hirayama, M.; Mitsui, A.; Yonemura, M.; Iba, H.; Kanno, R. High-power all-solid-state batteries using sulfide superionic conductors. *Nature Energy* **2016**, *1* (4), 16030.
- (13) Seino, Y.; Ota, T.; Takada, K.; Hayashi, A.; Tatsumisago, M. A sulphide lithium super ion conductor is superior to liquid ion conductors for use in rechargeable batteries. *Energy Environ. Sci.* **2014**, *7* (2), 627–631.
- (14) Long, L.; Wang, S.; Xiao, M.; Meng, Y. Polymer electrolytes for lithium polymer batteries. *J. Mater. Chem. A* **2016**, *4* (26), 10038–10069.
- (15) Xue, Z.; He, D.; Xie, X. Poly(ethylene oxide)-based electrolytes for lithium-ion batteries. *J. Mater. Chem. A* **2015**, *3* (38), 19218–19253.
- (16) Hiemenz, P. C.; Lodge, T. P. *Polymer Chemistry*, 2nd ed.; CRC Press: 2007.
- (17) Müller-Plathe, F.; van Gunsteren, W. F. Computer simulation of a polymer electrolyte: lithium iodide in amorphous poly (ethylene oxide). *J. Chem. Phys.* **1995**, *103* (11), 4745–4756.
- (18) Costa, L.; Gad, A. M.; Camino, G.; Cameron, G. G.; Qureshi, M. Y. Thermal and thermooxidative degradation of poly(ethylene oxide)-metal salt complexes. *Macromolecules* **1992**, *25* (20), 5512–5518.
- (19) Gordon Cameron, G.; Ingram, M. D.; Younus Qureshi, M.; Gearing, H. M.; Costa, L.; Camino, G. The thermal degradation of poly(ethylene oxide) and its complex with NaCNS. *Eur. Polym. J.* **1989**, *25* (7), 779–784.
- (20) Hu, M.; Pang, X. L.; Zhou, Z. Recent progress in high-voltage lithium ion batteries. *J. Power Sources* **2013**, *237*, 229–242.
- (21) Choi, N. S.; Han, J. G.; Ha, S. Y.; Park, I.; Back, C. K. Recent advances in the electrolytes for interfacial stability of high-voltage cathodes in lithium-ion batteries. *RSC Adv.* **2015**, *5* (4), 2732–2748.
- (22) Hu, P.; Chai, J.; Duan, Y.; Liu, Z.; Cui, G.; Chen, L. Progress in nitrile-based polymer electrolytes for high performance lithium batteries. *J. Mater. Chem. A* **2016**, *4* (26), 10070–10083.
- (23) Ramesh, S.; Ng, H. An investigation on PAN-PVC-LiTFSI based polymer electrolytes system. *Solid State Ionics* **2011**, *192* (1), 2–5.
- (24) Li, J.; Huang, X.; Chen, L. X-Ray Diffraction and Vibrational Spectroscopic Studies on PAN-LiTFSI Polymer Electrolytes. *J. Electrochem. Soc.* **2000**, *147* (7), 2653–2657.
- (25) Huang, B.; Wang, Z.; Li, G.; Huang, H.; Xue, R.; Chen, L.; Wang, F. Lithium ion conduction in polymer electrolytes based on PAN. *Solid State Ionics* **1996**, *85* (1), 79–84.
- (26) Yaroslavtseva, T. V.; Bushkova, O. V. Glass transitions and ionic conductivity in a poly(butadiene-acrylonitrile)-LiAsF<sub>6</sub> system. *Electrochim. Acta* **2011**, *57*, 212–219.
- (27) Li, Z.; Zhao, Y.; Tenhaeff, W. E. 5 V Stable Nitrile-Bearing Polymer Electrolyte with Aliphatic Segment as Internal Plasticizer. *ACS Applied Energy Materials* **2019**, *2*, 3264.
- (28) Braun, D.; Haufe, A.; Leiß, D.; Hellmann, G. P. Strain-induced crystallisation and miscibility behaviour of hydrogenated nitrile rubbers. *Angew. Makromol. Chem.* **1992**, *202* (1), 143–158.
- (29) Alcock, B.; Olafsen, K.; Huse, J.; Grytten, F. The low temperature crystallization of hydrogenated nitrile butadiene rubber (HNBR). *Polym. Test.* **2018**, *66*, 228–234.
- (30) Pal, P.; Ghosh, A. Charge carrier dynamics in PMMA-LiClO<sub>4</sub> based polymer electrolytes plasticized with different plasticizers. *J. Appl. Phys.* **2017**, *122* (1), 015101.
- (31) Dam, T.; Ghosh, A. Ion Conduction Phenomenon and Electrochemical Performance of Gel Polymer Electrolyte in EDLC Containing Blend Polymer Host, Ionic Liquid, and Mixed Carbonate Plasticizers. *J. Phys. Chem. C* **2018**, *122* (48), 27214–27223.
- (32) Goodenough, J. B.; Kim, Y. Challenges for Rechargeable Li Batteries. *Chem. Mater.* **2010**, *22* (3), 587–603.
- (33) SaÇan, M. T.; Özkul, M.; Erdem, S. S. Physico-chemical properties of PCDD/PCDFs and phthalate esters AU - SaÇan, M. T. SAR and QSAR in *Environmental Research* **2005**, *16* (5), 443–459.
- (34) Wang, B.; Qu, Q. T.; Xia, Q.; Wu, Y. P.; Li, X.; Gan, C. L.; van Ree, T. Effects of 3,5-bis(trifluoromethyl)benzeneboronic acid as an additive on electrochemical performance of propylene carbonate-based electrolytes for lithium ion batteries. *Electrochim. Acta* **2008**, *54* (2), 816–820.
- (35) Xu, K. Electrolytes and Interphases in Li-Ion Batteries and Beyond. *Chem. Rev.* **2014**, *114* (23), 11503–11618.
- (36) Lide, D. R. *CRC handbook of chemistry and physics*; CRC press: 2004; Vol. 85.
- (37) Yang, D.; Tian, M.; Dong, Y.; Liu, H.; Yu, Y.; Zhang, L. Disclosed dielectric and electromechanical properties of hydrogenated nitrile-butadiene dielectric elastomer. *Smart Mater. Struct.* **2012**, *21* (3), 035017.
- (38) Rahman, M.; Brazel, C. S. The plasticizer market: an assessment of traditional plasticizers and research trends to meet new challenges. *Prog. Polym. Sci.* **2004**, *29* (12), 1223–1248.
- (39) Walker, C. W.; Salomon, M. Improvement of Ionic Conductivity in Plasticized PEO-Based Solid Polymer Electrolytes. *J. Electrochem. Soc.* **1993**, *140* (12), 3409–3412.
- (40) Michael, M. S.; Jacob, M. M. E.; Prabakaran, S. R. S.; Radhakrishna, S. Enhanced lithium ion transport in PEO-based solid polymer electrolytes employing a novel class of plasticizers. *Solid State Ionics* **1997**, *98* (3–4), 167–174.
- (41) Rajendran, S.; Mahendran, O.; Kannan, R. Investigations on poly(methyl methacrylate)-poly(ethylene oxide) hybrid polymer electrolytes with dioctyl phthalate, dimethyl phthalate and diethyl phthalate as plasticizers. *J. Solid State Electrochem.* **2002**, *6* (8), 560–564.
- (42) Rey, I.; Johansson, P.; Lindgren, J.; Lassègues, J. C.; Grondin, J.; Servant, L. Spectroscopic and Theoretical Study of (CF<sub>3</sub>SO<sub>2</sub>)<sub>2</sub>N-(TFSI-) and (CF<sub>3</sub>SO<sub>2</sub>)<sub>2</sub>NH (HTFSI). *J. Phys. Chem. A* **1998**, *102* (19), 3249–3258.
- (43) Lin-Vien, D.; Colthup, N. B.; Fateley, W. G.; Grasselli, J. G. *The handbook of infrared and Raman characteristic frequencies of organic molecules*; Elsevier: 1991.
- (44) Sim, L. N.; Majid, S. R.; Arof, A. K. FTIR studies of PEMA/PVdF-HFP blend polymer electrolyte system incorporated with LiCF<sub>3</sub>SO<sub>3</sub> salt. *Vib. Spectrosc.* **2012**, *58*, 57–66.
- (45) Pfeiffer, H. G.; Liebhaufsky, H. A. The origins of Beer's law. *J. Chem. Educ.* **1951**, *28* (3), 123.
- (46) Meyer, W. H. Polymer electrolytes for lithium-ion batteries. *Adv. Mater.* **1998**, *10* (6), 439–448.
- (47) Vincent, C. A. Polymer electrolytes. *Prog. Solid State Chem.* **1987**, *17* (3), 145–261.
- (48) Bailey, F., Jr; Koleske, J. *Poly (ethylene oxide), Properties of Poly (ethylene oxide)*; Academic Press: New York, 1976.
- (49) Diederichsen, K. M.; Buss, H. G.; McCloskey, B. D. The compensation effect in the Vogel-Tammann-Fulcher (VTF) equation for polymer-based electrolytes. *Macromolecules* **2017**, *50* (10), 3831–3840.

- (50) Kalnaus, S.; Sabau, A. S.; Tenhaeff, W. E.; Dudney, N. J.; Daniel, C. Design of composite polymer electrolytes for Li ion batteries based on mechanical stability criteria. *J. Power Sources* **2012**, *201*, 280–287.
- (51) Kalnaus, S.; Tenhaeff, W. E.; Sakamoto, J.; Sabau, A. S.; Daniel, C.; Dudney, N. J. Analysis of composite electrolytes with sintered reinforcement structure for energy storage applications. *J. Power Sources* **2013**, *241*, 178–185.
- (52) Shobha, H. K.; Kishore, K. Structural expressions of long-chain esters on their plasticizing behavior in poly(vinyl chloride). *Macromolecules* **1992**, *25* (25), 6765–6769.
- (53) Liu, X.; Stolarov, S. I.; Denlinger, M.; Masias, A.; Snyder, K. Comprehensive calorimetry of the thermally-induced failure of a lithium ion battery. *J. Power Sources* **2015**, *280*, 516–525.
- (54) Bouchet, R.; Lascaud, S.; Rosso, M. An EIS study of the anode Li/PEO-LiTFSI of a Li polymer battery. *J. Electrochem. Soc.* **2003**, *150* (10), A1385–A1389.
- (55) Qian, X. M.; Gu, N. Y.; Cheng, Z. L.; Yang, X. R.; Wang, E. K.; Dong, S. J. Impedance study of (PEO)(10)LiClO<sub>4</sub>-Al<sub>2</sub>O<sub>3</sub> composite polymer electrolyte with blocking electrodes. *Electrochim. Acta* **2001**, *46* (12), 1829–1836.
- (56) Ratner, M. A.; Shriver, D. F. Ion transport in solvent-free polymers. *Chem. Rev.* **1988**, *88* (1), 109–124.
- (57) Devaux, D.; Bouchet, R.; Glé, D.; Denoyel, R. Mechanism of ion transport in PEO/LiTFSI complexes: Effect of temperature, molecular weight and end groups. *Solid State Ionics* **2012**, *227*, 119–127.
- (58) MacCallum, J. R.; Vincent, C. A. *Polymer electrolyte reviews*; Springer Science & Business Media: 1989; Vol. 2.
- (59) Dahbi, M.; Ghamouss, F.; Tran-Van, F.; Lemordant, D.; Anouti, M. Comparative study of EC/DMC LiTFSI and LiPF<sub>6</sub> electrolytes for electrochemical storage. *J. Power Sources* **2011**, *196* (22), 9743–9750.
- (60) Matsuda, Y.; Morita, M.; Kosaka, K. Conductivity of the Mixed Organic Electrolyte Containing Propylene Carbonate and 1,2-Dimethoxyethane. *J. Electrochem. Soc.* **1983**, *130* (1), 101–104.
- (61) Xu, K. Nonaqueous liquid electrolytes for lithium-based rechargeable batteries. *Chem. Rev.* **2004**, *104* (10), 4303–4417.
- (62) Tenhaeff, W. E.; Perry, K. A.; Dudney, N. J. Impedance Characterization of Li Ion Transport at the Interface between Laminated Ceramic and Polymeric Electrolytes. *J. Electrochem. Soc.* **2012**, *159* (12), A2118–A2123.
- (63) Diederichsen, K. M.; McShane, E. J.; McCloskey, B. D. Promising Routes to a High Li<sup>+</sup> Transference Number Electrolyte for Lithium Ion Batteries. *ACS Energy Letters* **2017**, *2* (11), 2563–2575.
- (64) Doyle, M.; Fuller, T. F.; Newman, J. The importance of the lithium ion transference number in lithium/polymer cells. *Electrochim. Acta* **1994**, *39* (13), 2073–2081.
- (65) Doyle, M.; Newman, J. Analysis of transference number measurements based on the potentiostatic polarization of solid polymer electrolytes. *J. Electrochem. Soc.* **1995**, *142* (10), 3465–3468.
- (66) Bruce, P. G.; Vincent, C. A. Steady state current flow in solid binary electrolyte cells. *J. Electroanal. Chem. Interfacial Electrochem.* **1987**, *225* (1), 1–17.
- (67) Evans, J.; Vincent, C. A.; Bruce, P. G. Electrochemical measurement of transference numbers in polymer electrolytes. *Polymer* **1987**, *28* (13), 2324–2328.
- (68) Cameron, G. G.; Harvie, J. L.; Ingram, M. D. The steady state current and transference number measurements in polymer electrolytes. *Solid State Ionics* **1989**, *34* (1), 65–68.
- (69) Zugmann, S.; Fleischmann, M.; Amereller, M.; Gschwind, R. M.; Wiemhöfer, H. D.; Gores, H. J. Measurement of transference numbers for lithium ion electrolytes via four different methods, a comparative study. *Electrochim. Acta* **2011**, *56* (11), 3926–3933.
- (70) Hiller, M. M.; Joost, M.; Gores, H. J.; Passerini, S.; Wiemhöfer, H. D. The influence of interface polarization on the determination of lithium transference numbers of salt in polyethylene oxide electrolytes. *Electrochim. Acta* **2013**, *114*, 21–29.
- (71) Edman, L.; Doeff, M. M.; Ferry, A.; Kerr, J.; De Jonghe, L. C. Transport Properties of the Solid Polymer Electrolyte System P(EO)<sub>n</sub>LiTFSI. *J. Phys. Chem. B* **2000**, *104* (15), 3476–3480.
- (72) Nitta, N.; Wu, F.; Lee, J. T.; Yushin, G. Li-ion battery materials: present and future. *Mater. Today* **2015**, *18* (5), 252–264.
- (73) Brissot, C.; Rosso, M.; Chazalviel, J. N.; Lascaud, S. Dendritic growth mechanisms in lithium/polymer cells. *J. Power Sources* **1999**, *81*–82, 925–929.
- (74) Zhou, W.; Wang, Z.; Pu, Y.; Li, Y.; Xin, S.; Li, X.; Chen, J.; Goodenough, J. B. Double-Layer Polymer Electrolyte for High-Voltage All-Solid-State Rechargeable Batteries. *Adv. Mater.* **2019**, *31* (4), 1805574.